Synthesis, crystal structure, magnetic, spectroscopic, and theoretical investigations of two new nitronyl-nitroxide complexes

Cristian Andrei Spinu, Céline Pichon, Gabriela Ionita, Teodora Mocanu, Sergiu Calancea, Mihai Raduca, Jean-Pascal Sutter, Mihaela Hillebrand, Marius Andruh

Synthesis, crystal structure, magnetic, spectroscopic, and theoretical investigations of two new nitronyl-nitroxide complexes

Cristian Andrei Spinu[a], Céline Pichon[b], Gabriela Ionita[c], Teodora Mocanu[a,c], Sergiu Calancea[a,e], Mihai Raduca[a], Jean-Pascal Sutter*[b], Mihaela Hillebrand*[f] and Marius Andruh*[a]

[a]*Inorganic Chemistry Laboratory, Faculty of Chemistry, University of Bucharest, Str. Dumbrava Rosie 23, 020464-Bucharest, Romania; e-mail: marius.andruh@dnt.ro*
[b]*Laboratoire de Chimie de Coordination du CNRS (LCC), Université de Toulouse, CNRS, Toulouse, France; e-mail: sutter@lcc-toulouse.fr*
[c]*"Ilie Murgulescu" Institute of Physical Chemistry, Romanian Academy, Splaiul Independentei 202, Bucharest-060021, Romania*
[e]*Moldova State University, MD-2009-Chisinau, Faculty of Chemistry and Chemical Technology, Moldova*
[f]*Physical Chemistry Department, Faculty of Chemistry, University of Bucharest, Bd. Elisabeta 4-12, 030018-Bucharest, Romania; E-mail: mihaela.hillebrand@gmail.com*

ABSTRACT

Two mononuclear complexes $[(Et_3NH)[M(hfac)_2L]$ (M = Ni, **1** Zn, **2**) have been synthesized using a nitronyl-nitroxide radical substituted nitrophenol, i.e., 2-(2-Hydroxy-3-methoxy-5-nitrophenyl)-4,4,5,5-tetramethyl-4,5-dihydro-1*H*-imidazol-3-oxide-1-oxyl, HL, as a proligand. The crystal structures of the two compounds have been solved and indicate an octahedral coordination geometry of the metal ions. The magnetic behavior for compound **1** is characterized by a strong antiferromagnetic metal-radical interaction (J = -351 ± 1 cm^{-1}; $\boldsymbol{H} = -J\boldsymbol{S}_{Ni}\boldsymbol{S}_{Rad}$). This exchange interaction was rationalized by DFT calculations. The EPR spectra recorded both in solution and solid state at 120 K confirm the S = ½ ground state for compound **1**.

1. INTRODUCTION

A large family of molecular magnetic materials consists of heterospin complexes generated by *d* or *f* metal ions and paramagnetic organic radicals acting as ligands [1]. The most popular radicals are the nitronyl-nitroxides (Nit), which are readily obtained, starting from aldehydes, following or adapting Ullman's synthetic approach [2]. The rich diversity of nitronyl-nitroxide ligands arises from the availability of a very large number of mono- and polyaldehydes, as well as from the possibility to decorate the nitronyl-nitroxide platform with other coordinating groups (preexisting in the staring aldehydes), which play an important role on the nuclearities and spin topologies of the resulting systems [3]. The family of magnetic materials constructed using paramagnetic organic ligands has been recently extended with polynuclear complexes containing two different metal ions, both paramagnetic [4]. Most of these heterotrispin complexes contain 3*d* and 4*f* metal ions. The exchange interactions between 2*p* radicals and paramagnetic metal ions vary between large limits, from strong antiferromagnetic to strong ferromagnetic couplings, [1, 3] and usually the 2*p*-n*d* couplings are stronger than those involving lanthanides. Magneto-structural studies highlight the factors influencing the nature and strength of the exchange interactions [1]. The geometric parameters, at the level of aminoxyl-metal bond, influence the orientation of the magnetic orbitals, π* (Nit) and *d* or *f*, and, consequently, their overlap or orthogonality.

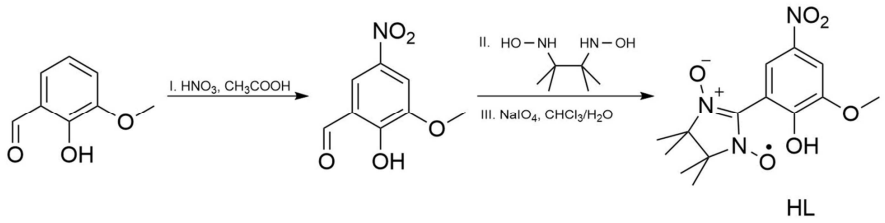

Scheme 1. Synthesis of the paramagnetic ligand.

Surprisingly, in spite of their simplicity and popularity in coordination chemistry, *o*-vanillin [5] and its substituted derivatives have been rarely employed as precursors for nitronyl-nitroxide ligands. To the best of our knowledge, there is only one report on the synthesis of the nitronyl-nitroxide obtained from *o*-vanillin [6], but this radical has never been employed as a ligand. This might be related to the poor yield of the synthesis of the radical derived from *o*-vanillin. A more convenient method consists in employment of derivatives that contain a substituent in *para* position with respect to the phenolic group, preventing the formation of by-products during the oxidation step with sodium periodate. The nitro derivative can be easily synthesized from *o*-vanillin and nitric acid and is subsequently transformed into the desired radical, HL (Scheme 1) [7]. In this paper we report on the synthesis, crystal structure

and physical properties of two new mononuclear compounds, which contains L^- as a ligand: $(Et_3NH)[M(hfac)_2L]$ (M = Ni, Zn).

2. EXPERIMENTAL PART

2.1. General procedures

Synthesis of 2,3-dimethyl-2,3-dinitrobutane and 2-hydroxy-3-methoxy-5-nitrobenzaldehyde were performed according to the reported procedures [8,9]. All other reagents and solvents were commercially purchased and used without any further purification, if not stated otherwise. IR spectra were recorded on a FTIR Bruker Tensor V-37 spectrophotometer (KBr pellets) in the range of 4000–400 cm^{-1}. UV−Vis diffuse reflectance spectra were recorded on a JASCO V-670 spectrophotometer on undiluted samples in the range 200 - 1800 nm. Elemental analyses (C, H, N) were performed on a EuroEA Elemental Analyzer. All Nuclear Magnetic Resonance (^1H and ^{13}C NMR) measurements were recorded on a Bruker 500 MHz spectrometer, at 25°C in $CDCl_3$. The X-ray powder diffraction measurements were carried out on a Proto AXRD Benchtop using Cu-Kα radiation with a wavelength of 1.54059 Å in the range 5-35º (2θ). The metal ratio in the compound $[Ni_{0.2}Zn_{0.8}]$ was determined using the element energy dispersive spectroscopy (EDS) system (Smart Insight AMETEK), coupled with a Nova NanoSEM 630 Scanning Electron Microscope (FEI Company, Hillsboro, OR, USA). The EDAX spectrum was acquired at an acceleration voltage of 18 kV, with a working distance of 5 mm and 30000x magnification.

The EPR spectra were recorded with a JEOL FA 100 spectrometer equipped with a VT controller using the following setting: microwave power 1 mW, frequency 100 kHz, sweep field 2000 G, center field 3221.8 G, sweep time 1800 s, modulation width 2 G.

The magnetic field calibration was performed with a DPPH (diphenylpicrylhydrazyl) standard marker, exhibiting a narrow EPR line at g = 2.0036. The EPR spectra of Zn and Ni complexes and their mixture (molar ratio Ni/Zn 2:8) were recorded by filling a glass capillary that was placed in an EPR tube. For solution samples, the complexes or nitronyl-nitroxide radical were dissolved in CH_2Cl_2. The oxygen has been removed from solution by bubbling Ar gas. Frozen spectra were recorded at 120 K. The a_N values of nitronyl-nitroxide radical were obtained by simulation of experimental spectra using Winsim program.

Magnetic measurements for **1** were carried out with a Quantum Design MPMS 5S SQUID magnetometer in the temperature range 2−300 K. The crystalline powder of the complex was mixed with grease in a gelatin capsule. The temperature dependence of the magnetization was

collected in an applied field of 1kOe and the isothermal field dependence of the magnetizations were collected up to 5 T. The molar susceptibility (χ_M) was corrected for sample holder, grease and for the diamagnetic contribution of all the atoms by using Pascal's tables. Possible slow relaxation of the magnetization was examined by AC susceptibility collected in zero field and with applied fields.

Table 1. Crystallographic data, details of data collection and structure refinement parameters for compounds **1** and **2**.

Complex	**1**	**2**
Empirical formula	$C_{30}H_{35}N_4NiO_{10}F_{12}$	$C_{30}H_{35}N_4ZnO_{10}F_{12}$
Formula weight	898.33	904.99
Temperature (K)	293.15	293.15
Crystal system	Monoclinic	Monoclinic
Space group	$P2_1/c$	$P2_1/c$
a (Å)	20.2955(15)	20.4327(7)
b (Å)	9.6043(6)	9.5457(2)
c (Å)	21.5013(15)	21.5624(7)
α (°)	90	90
β (°)	110.349(5)	111.461(4)
γ (°)	90	90
Volume (Å^3)	3929.6(5)	3914.0(2)
Z	4	4
D_c (g/cm^3)	1.518	1.536
Absorption coefficient (mm^{-1})	0.607	0.741
F(000)	1836.04	1844.0
Θ range for data collection (°)	1.93 to 24.999	2.03 to 30.783
Index ranges	-24≤h≤24, -11≤k≤11, -25≤l≤25	-25≤h≤26, -10≤k≤13, -26≤l≤27
Reflections collected	40888	39190
Independent reflections [R_{int}]	6936 [R_{int} = 0.1320]	9656 [R_{int} = 0.0337]
Completeness to Θ full (%)	100.0	100.0
Data/restraints/parameters	6936/18/642	9656/25/654
Goodness of fit on F^2	1.039	1.015
R_1, wR_2 [$I > 2\sigma I$]	0.0596, 0.1108	0.0378, 0.0984
R_1, wR_2 (all data)	0.1414, 0.1476	0.0680, 0.1111
Largest diff. peak/hole (Å^3)	0.23/-0.34	0.28/-0.24

2.2. X-Ray data collection and crystal structure refinement

Crystallographic data were collected on a STOE IPDS II diffractometer for **1** and on a Rigaku XtaLAB Synergy, single source at offset/far, HyPix diffractometer for **2**, using a graphite-monochromated Mo K_α radiation source (λ = 0.71073Å). The structures were solved by direct methods and refined by full-matrix least squares techniques based on F^2. The non-H atoms were refined with anisotropic displacement parameters. Hydrogen atoms were placed in fixed, idealized positions and refined as rigidly bonded to the corresponding atoms. Calculations were performed using SHELXT and SHELXL-2015 crystallographic software

packages [10] A summary of the crystallographic data and the structure refinement is given in Tables 1 and S1 CCDC reference numbers: 2032386 (**1**); 2032384 (**2**); 2032385 ($Ni_{0.2}Zn_{0.8}$).

2.3. Synthesis of 2,3-bis(hydroxylamino)-2,3-dimethylbutan

The synthesis of this ligand was adapted from reported procedure [11]. A solution of $HgCl_2$ (1.028 g, 3.78 mmol) in 50 mL of water was added over strips of aluminum foil (1.534 g, 57.82 mmol). The mixture was stirred for 2 minutes after which the liquid was removed with a pipet. The amalgamated aluminum was cooled keeping it in a glassware immersed in an ice bath and then a solution of 2,3-dimethyl-2,3-dinitrobutane (2 g, 11.36 mmol) in 60 mL of tetrahydrofuran (THF) and 6 mL of H_2O were added sequentially. The reaction is left to evolve 1 h under strong stirring at low temperature followed by filtration on a pad of celite which was washed with another 60 mL of THF. The solvents from the filtered solution were removed under vacuum, to obtain a white precipitate. The precipitate was dissolved in 25 mL of $CHCl_3$ over which 25 mL of diethyl ether were added. The solution was left overnight in the freezer to form the product as a white crystalline powder, 0.555 g, yield 33 %. The product was stored dried in a fridge. Anal. Calcd. for $C_6H_{16}N_2O_2$ (%): C, 48.63; H, 10.88; N, 18.90. Found: C, 48.68; H, 10.90; N, 18.96. Selected IR peaks (cm^{-1}): 3368 (s), 3287 (s), 3252 (vs), 2988 (vs), 2943 (s), 1479 (m), 1452 (m), 1425 (m), 1404 (s), 1387 (s), 1375 (s), 1358 (m), 1261 (m), 1177 (m), 1146 (s), 1080 (m), 1036 (m), 989 (w), 951 (m), 932 (w), 905 (s), 853 (w), 791 (w), 690 (m), 609 (w), 494 (w), 441(w). ^{1}H-RMN (500.13 MHz, $CDCl_3$, δ ppm): 1.19 (s, 12 H, C**H$_3$**-); ^{13}C-RMN (125.77 MHz, $CDCl_3$, δ ppm): 62.97 (CH_3-**C**-CH_3), 20.81(**C**H_3-).

2.4. Synthesis of 2-(2-Hydroxy-3-methoxy-5-nitrophenyl)-4,4,5,5-tetramethyl-4,5-dihydro-1H-imidazol-3-oxide-1-oxyl (HL)

The synthesis of this ligand was devised and adapted from reported procedures [2,7]. To a solution of 2,3-bis(hydroxylamino)-2,3-dimethylbutan (1.523 g, 10.288 mmol) in 50 mL of MeOH, another solution of 2-hydroxy-3-methoxy-5-nitrobenzaldehyde (1.843 g, 9.353 mmol) in 75 mL of MeOH was added. The mixture was refluxed for 4 h followed by the evaporation of the solvent under vacuum. Over the yellow intermediate, 100 mL of $CHCl_3$ was added and the solution was ice cooled then, a solution of $NaIO_4$ (2.002 g, 9.353 mmol) in 100 mL of water was added. The obtained biphasic system was placed under strong stirring and the reaction left to evolve at 0 °C for 15 min and then at 25 °C for 45 min. The organic phase was isolated using a separatory funnel and dried with $MgSO_4$. The solvent was

evaporated under vacuum to obtain the crude blue product which was recrystallized four times from a mixture of CH_2Cl_2 : diethyl ether, 1 : 1 volumetric ratio, to obtain the pure blue product, 1.391 g, yield 46%. Anal. Calcd. for $C_{14}H_{18}N_3O_6$ (%): C, 51.85; H, 5.59; N, 12.97. Found: C, 52.27; H, 5.41; N, 12.75. Selected IR peaks (cm^{-1}): 1581 (w), 1530 (m), 1462 (m), 1429 (m), 1394 (m), 1373 (w), 1350 (vs), 1258 (m), 1201 (w), 1163 (m), 1138 (w), 1105 (w), 1069 (w), 923 (w), 885 (w), 739 (m), 457 (m). UV-Vis (nm): 362, 571.

2.5. Synthesis of $(Et_3NH)[NiL(hfac)_2]$, 1

$Ni(hfac)_2 \cdot 2H_2O$ (0.060 g, 0.1852 mmol) was dissolved in 15 mL of heptane and refluxed for 30 min. Then, after cooling down the solution , another 15 mL of CH_2Cl_2 solution containing HL (0.094 g, 0.1852 mmol) and 1 drop of triethylamine was added. The solution is refluxed another 30 min, cooled down and filtered. After allowing the solvent to slowly evaporate for three days, needle shaped violet crystals of the product were obtained, 0.125 g, yield 75%. Anal. Calcd. for $C_{30}H_{35}F_{12}N_4O_{10}Ni$ (%): C, 40.11; H, 3.93; N, 6.24; Found: C, 39.61; H, 4.13; N, 5.87. Selected IR peaks (cm^{-1}): 1657 (s), 1645 (s), 1600 (w), 1555 (m), 1524 (s), 1502 (s), 1396 (w), 1364 (m), 1310 (s), 1256 (vs), 1234 (m), 1204 (vs) 1148 (vs), 1097 (m), 1070 (w), 870 (w), 793 (m), 673 (m), 586 (w). UV-Vis (nm): 413, 571, 751, 1142.

2.6. Synthesis of $(Et_3NH)[ZnL(hfac)_2]$, 2

$Zn(hfac)_2 \cdot 2H_2O$ (0.047 g, 0.0926 mmol) was dissolved in 7 mL of heptane and refluxed for 30 min. Then, after cooling down the solution, another 7 mL of CH_2Cl_2 solution containing HL (0.030 g, 0.0926 mmol) and 1 drop of triethylamine was added. The solution is refluxed another 30 min, cooled down and filtered. After allowing the solvent to slowly evaporate for three days, needle shaped violet crystals of the product were obtained, 0.046 g, yield 55%. Anal. Calcd. for $C_{30}H_{35}F_{12}N_4O_{10}Zn$ (%): C, 39.82; H, 3.90; N, 6.19; Found: C, 40.33; H, 3.80; N, 6.06. Selected IR peaks (cm^{-1}): 1663 (m), 1649 (s), 1601 (m), 1557 (m), 1528 (s), 1504 (s), 1399 (w), 1366 (m), 1331 (m), 1310 (s), 1286 (m), 1256 (vs), 1234 (m), 1204 (s), 1144 (vs), 1096 (m), 1071 (w), 869 (w), 795 (m), 765 (w), 746 (w), 669 (m), 583 (w). UV-Vis (nm): 424, 584.

The molecular alloy, $[Ni_{0.2}Zn_{0.8}(L(hfac)_2]$, has been obtained by reacting the zinc and nickel salts in 1:4 molar ratio, in the same experimental conditions described above for compounds **1** and **2**. The powder X-Ray diffractogram is similar to those recorded for compounds **1** and **2** (Figure S3) The Ni:Zn molar ratio in the resulting alloy was confirmed by EDX measurements.

2.7. Computational details

The exchange coupling interaction was calculated by the DFT method using the Gaussian 09 program [12], considering two spin states, namely a low (S = 1/2 resulting from S_{Ni} = 1 and S_{Rad}= -1/2 spin states) and a high spin HS (S = 3/2 resulting from S_{Ni} = 1 and S_{Rad} = ½ spin states) one. The calculations were performed on the crystal geometry without further optimization. The energy of the low spin state, hereafter labeled as the Broken Symmetry (BS) state, was calculated by the fragment procedure as implemented in the Gaussian09 program and further checked for its stability. The calculations were performed using the basis set, TZVP [13], and three functionals, uB3LYP [14], uB3PW91 [15], and uM06 [16]. The EPR spectra of the two Ni and Zn complexes were firstly calculated using the same theoretical model and the crystal geometry, but considering literature data [17], we have also used a new basis set recommended for EPR, TZVP/ EPR-III, and a very simple one, 6-31g*. Taking into account the results obtained by these models, the DCM solution spectra were calculated using only the TZVP and the 6-31g* basis sets after the geometry optimization in the solvent.

3. RESULTS AND DISCUSSION

3.1. Description of the crystal structures

The new compounds, $(Et_3NH)[M(hfac)_2L]$ (M = Ni **1**, Zn **2**), have been synthesized by reacting the metal precursors, $[M(hfac)_2(H_2O)_2]$ with the paramagnetic proligand, HL, in the presence of triethylamine, which was added for the deprotonation of the phenolic group. The PXRD patterns for **1** and **2** confirm the purity of the crystalline phases (Figures S1 and S2). Since the two compounds are isostructural, only the crystal structure of **1** will be described in detail.

Its crystal structure consists of anionic complexes, $[Ni(hfac)_2L]^-$ (Figure 1) and organic cations, Et_3NH^+. The nickel ion shows an octahedral geometry, being coordinated by four oxygen atoms arising from the $hfac^-$ ligands and two others from L^- (one phenoxido and one aminoxyl oxygen). The Ni – O oxygen distances vary between 2.008(4) and 2.072(4) Å. The N-O bond within the aminoxyl group coordinated to Ni^{II} (1.305(5) Å) is longer than the one within the uncoordinated NO group (1.266(5) Å). The complex species are chiral and both enantiomers co-crystallize within the same crystal (Figure 2). The crystal structure of the complex anion in **2** is illustrated in Figure S4. Selected bond distances and angles for compounds **1** and **2** are collected in Table 2.

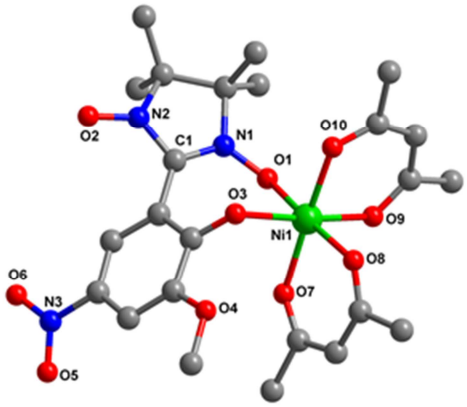

Figure 1. Molecular structure of the complex anion 1, along with the atom numbering scheme. Hydrogen and fluorine atoms have been omitted for clarity.

The diffuse reflectance spectra of the ligand and the two complexes are displayed in Figure 3. Compound **1** shows, apart from the bands arising from the organic ligands, two other bands which are due to the *d-d* transitions: $^3A_2 \rightarrow {}^3T_2$ (1122 nm) and $^3A_2 \rightarrow {}^3T_1$ (751 nm), assuming the O_h point group.

One single crystal from the [$Ni_{0.2}Zn_{0.8}$] sample was measured, and the structure was refined with occupation factors 0.2 for Ni and 0.8 for Zn (Table S1), in agreement with the EDX data. The powder X-Ray diffractogram for the alloy (Figure S3) is identical with those of **1** and **2**.

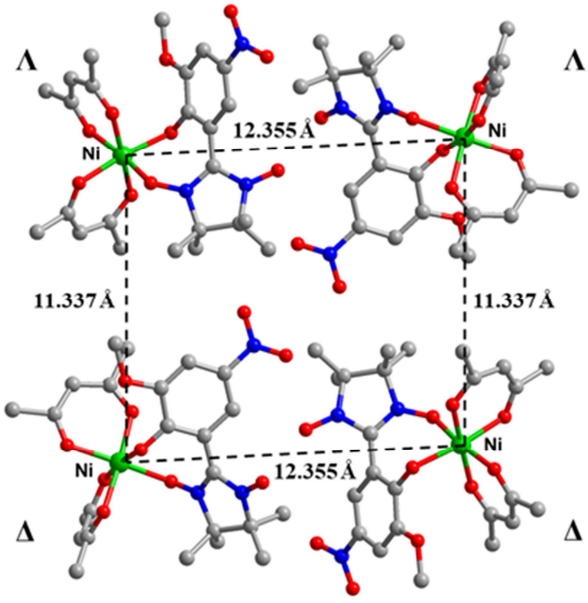

Figure 2. The packing diagram of **1** showing the closest distances between nickel metal ions and delta (Δ) or lambda (Λ) configurations of the metal centers.

Table 2. Selected bond distances (Å) and angles (º) for compounds **1** and **2**.

1		**2**	
Distances		Distances	
Ni1-O1	2.072(4)	Zn1-O1	2.204(2)
Ni1-O3	2.035(3)	Zn1-O3	2.035(1)
Ni1-O7	2.046(4)	Zn1-O7	2.095(2)
Ni1-O8	2.029(4)	Zn1-O8	2.089(2)
Ni1-O9	2.008(4)	Zn1-O9	2.051(2)
Ni1-O10	2.026(4)	Zn1-O10	2.090(2)
Angles		Angles	
O1-Ni1-O3	89.53(13)	O1-Zn1-O3	85.93(5)
O1-Ni1-O7	89.67(14)	O1-Zn1-O7	90.65(5)
O1-Ni1-O8	173.15(16)	O1-Zn1-O8	172.31(6)
O1-Ni1-O9	82.83(15)	O1-Zn1-O9	79.49(6)
O1-Ni1-O10	94.70(15)	O1-Zn1-O10	95.85(6)
O3-Ni1-O7	91.75(14)	O3-Zn1-O7	93.83(6)
O3-Ni1-O8	97.21(15)	O3-Zn1-O8	101.23(6)
O3-Ni1-O9	172.16(15)	O3-Zn1-O9	164.47(6)
O3-Ni1-O10	87.92(15)	O3-Zn1-O10	87.86(6)
O7-Ni1-O8	88.88(15)	O7-Zn1-O8	86.10(6)
O7-Ni1-O9	90.00(15)	O7-Zn1-O9	91.67(6)
O7-Ni1-O10	175.62(15)	O7-Zn1-O10	173.39(6)
O8-Ni1-O9	90.47(16)	O8-Zn1-O9	93.62(7)
O8-Ni1-O10	86.82(15)	O8-Zn1-O10	87.30(6)
O9-Ni1-O10	90.91(15)	O9-Zn1-O10	88.34(6)

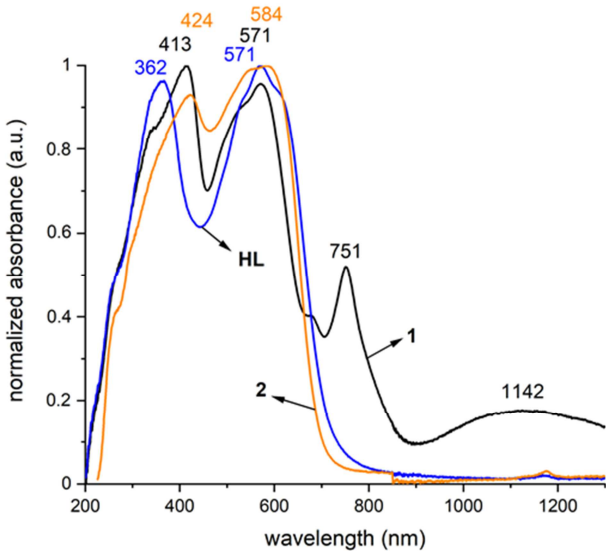

Figure 3. Diffuse reflectance spectra for HL and complexes **1** and **2**.

3.2. Magnetic properties of $(Et_3NH)[NiL(hfac)_2]$

The temperature dependence of the molar magnetic susceptibility, χ_M, for **1** has been investigated in the temperature range 2 – 300 K, and the field dependence of the magnetization was recorded at 2 K. The $\chi_M T$ vs. T and M vs. H plots are presented in Figure 4. The value of $\chi_M T$ found at 300 K is 0.70 $cm^3mol^{-1}K$, much smaller than the expected 1.375

$cm^3mol^{-1}K$ for the uncoupled S = 1 (Ni^{II}) and S =1/2 (Rad). Moreover, reducing the temperature, $\chi_M T$ decreases to 0.475 $cm^3mol^{-1}K$ at 120 K and below remains constant down to 2 K. Such a behavior is indicative for a strong antiferromagnetic Radical-Ni(II) interaction. The plateau reached below 150 K is the signature of a spin S = ½, resulting from the antiferromagnetic interaction between the spins S = ½ and 1. The resulting S = ½ ground state is further confirmed by the field dependence of the magnetization recorded at 2 K that tends to 1 μ_B at 5 T.

These magnetic data have been analysed using the HDvV Hamiltonain: $\boldsymbol{H} = -J\boldsymbol{S}_{Ni}\boldsymbol{S}_{Rad..}$ In order to avoid over-parameterization, only a mean g parameter was considered (the local g parameters were accurately determined by EPR spectroscopy, *vide infra*). The best fit yielded J = -351 ± 1 cm^{-1} and g = 2.185 ± 0.001.

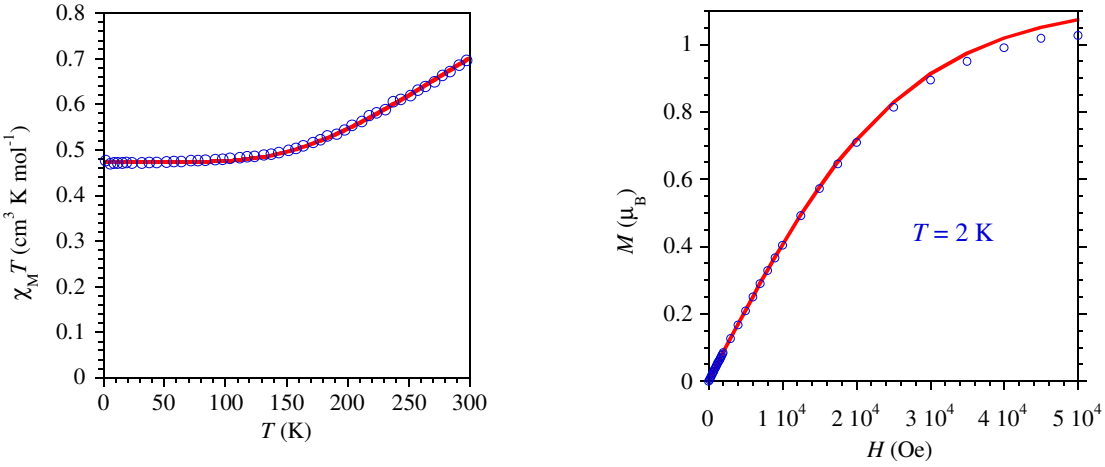

(a) **(b)**

Figure 4. Magnetic behavior for **1**: experimental (O) and calculated (—) (a) temperature dependence of the $\chi_M T$ and (b) magnetization vs. field

The nature of the exchange interactions (antiferro- and ferromagnetic) between nickel(II) and the aminoxyl group was subject of several magneto-structural correlations studies [18]. We recall here the most important conclusions, resulting from both experimental and theoretical investigations: (i) the coplanarity between the radical ring and the equatorial plane of the octahedral Ni^{II} ion favors a ferromagnetic coupling (the d_{x2-y2} and π^* radical orbital are orthogonal, while the overlap with the d_{z2} orbital is symmetry forbidden); (ii) the Ni-O-N-C dihedral angle as well as the Ni-O-N angle play a crucial on the overlap of the magnetic orbitals; (iii) large overlaps between the magnetic orbitals, and, consequently, strong antiferromagnetic interactions are favored by M-O-N-C dihedral angles close to 90º and by Ni-O-N angles close to 120º. These geometrical parameters for complex **1** (Ni1-O1-N1 =

126.1(3)º, Ni1-O1-N1-C1 = 58.6(6)º) suggest that the coupling between the nickel(II) ion and the radical must be antiferromagnetic and quite strong, in line with the experimental value. DFT calculations undertaken for **1** confirm the strong antiferromagnetic interaction between the paramagnetic centers, the ground state of the complex being the low spin state, *i.e.* the broken symmetry one. Starting from the spin Hamiltonian previously mentioned, $\boldsymbol{H} = -J\boldsymbol{S}_{Ni}\boldsymbol{S}_{Rad}$, the J value was obtained using the equation (1) [19]:

$$J = (E_{BS}-E_{HS})/(2\boldsymbol{S}_{Ni}\boldsymbol{S}_{Rad}+\boldsymbol{S}_{Rad}) \qquad (1)$$

The results presented in Table 3 are in agreement with the experimental value, J = -351 ± 1 (cm^{-1}). It can also be remarked that the three functionals used lead to quite similar results. As can be seen in Figure 5a and b, in both states, BS and HS, the spin densities are localized on the nickel ion and on the NO groups of the nitronyl-nitroxide radical, explaining the EPR spectra, *vide infra*.

Table 3. Calculated J values (cm^{-1}) for compound **1**.

Functional	Eq.(1)
uB3LYP	-400.53
uB3PW91	-398.23
uM06	-408.51

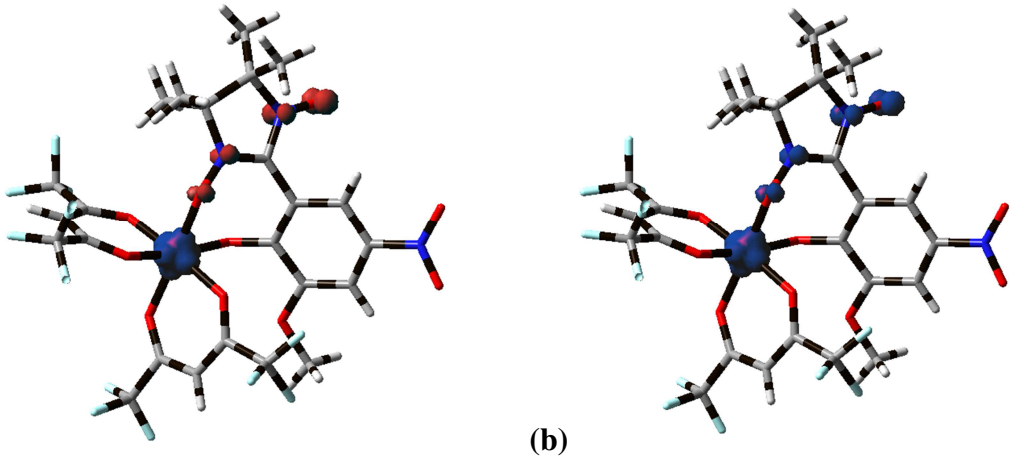

(a) **(b)**

Figure 5. Spin density (0.04) isosurfaces (0.04 $e^-/(a.u.)^3$) : a) BS state; b) HS state.

3.3 EPR spectra

The EPR spectra of the three paramagnetic compounds, the two complexes **1** and **2** and the nitronyl-nitroxide radical, were recorded both at room temperature, 293 K and at 120 K. The

spectrum of HL in CH_2Cl_2 at room temperature is displayed in Figure S5 and presents the known features of nitronyl-nitroxide radicals with a *g* factor of 2.0053 and a five line spectrum due to the hyperfine splitting (hfs) of two quasi-equivalent nitrogen atoms; the values obtained by simulation are a_{N1} = 7.40 G, a_{N2} = 7.55 G. The EPR spectrum recorded at 120 K indicates a restricted motion (Figure S5c).

The EPR spectra of the two complexes and their mixture, recorded in CH_2Cl_2 are plotted in Figure 6. At room temperature, the spectrum of the nickel complex, **1** , (Figure 6a), presents only the signal of the organic radical (*g* = 2.0053); at 120 K, the spectrum consists of two signals, a strong one characterized by *g* = 2.2751, and a very weak signal at *g*= 2.0051; the first signal is characteristic to a paramagnetic species with the electron localized on the nickel center [20] while the weak one is due to the organic radical. As expected, at both temperatures the spectrum of complex **2** presents only a single signal belonging to the organic radical the spectrum is unresolved at low temperature due to a strong broadening of the lines , but the *g* value is not influenced by temperature (293 K, *g* = 2.0055; 120 K, *g* = 2.0051). The isodensity spin surface displayed in Figure S6 reflects this behavior, the spin density being localized only on the NO groups. The assignment of the EPR spectra of **1** and **2** is verified by the spectra d and e in Figure 6; where it can be seen that the presence of the nickel ion determines the appearance at 120 K of the very weak signal at *g* = 2.2761 previously assigned to the spin localization on nickel and a large signal at g = 2.0056 corresponding to complex **2**. The strong signal of nitronyl-nitroxide fragment observed at 120 K is due to the excess of zinc complex in solution.

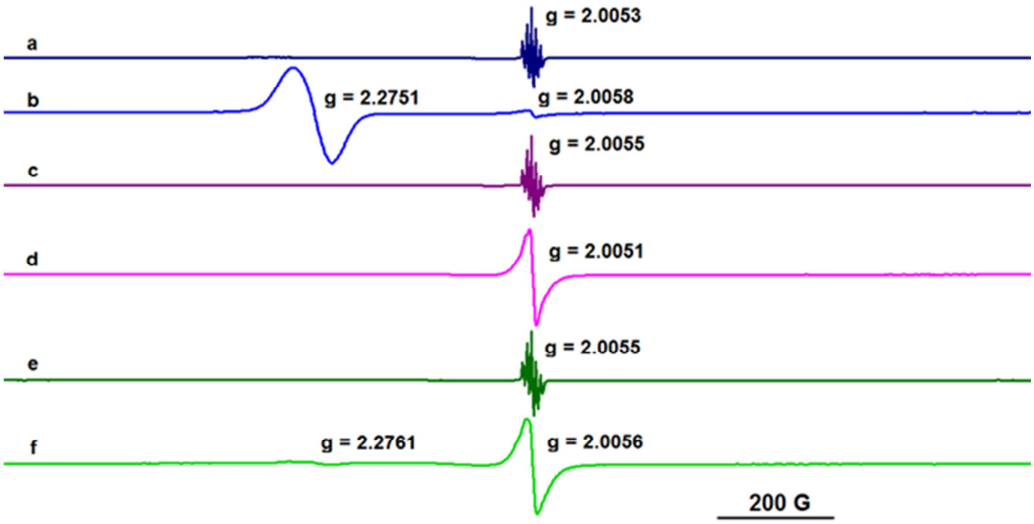

Figure 6. The EPR spectra in DCM recorded at 293 and 120 K: a) **1** at 293 K; b) **1** at 120 K ; c) **2** at 293 K; d) **2** at 120 K; e) $Ni_{0.2}Zn_{0.8}$ at 293 K; f) $Ni_{02}Zn_{0.8}$ at 120 K.

The same behavior is illustrated by the EPR spectra recorded in solid state (Figure 7), for **1**, **2** and the molecular alloy [$Ni_{0.2}Zn_{0.8}$]. Although the isostructural zinc derivative, **2**, is not a diamagnetic host for **1**, and cannot suppress all the dipolar interactions, some information can be extracted by comparing all these spectra.

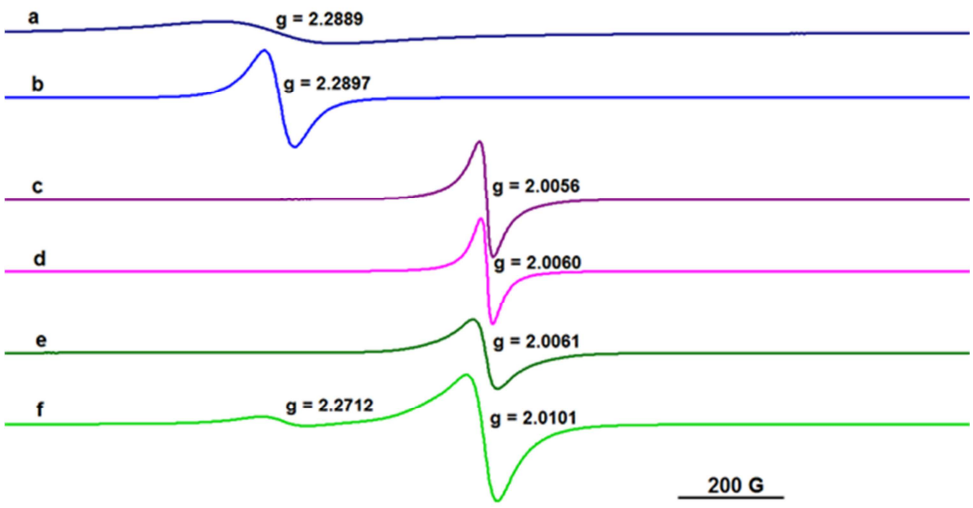

Figure 7. Solid state EPR spectra of: a) **1** at 293 K; b) **1** at 120 K; c) **2** at 293 K; d) **2** at 120 K; e) $Ni_{0.2}Zn_{0.8}$ at 293 K; f) $Ni_{0.2}Zn_{0.8}$ at 120 K.

At room temperature compound **1** shows only a broad and weak feature at g = 2.2889, which is due to the S = ½ state. As expected, this signal becomes stronger at 120 K, where only the spin state S = ½ is populated (Figure 7b). The spectra of the zinc derivative do not change with the temperature (Figure 7c,d). The molecular alloy of **1** and **2** shows at room temperature (Figure 7e) only one signal (g = 2.0061) arising from complex **2**; at 120 K (Figure 7f) two signals are observed: g = 2.0102 (due to complex **2**) and g = 2.2712 (S = ½ ground state of **1**).

The hyperfine splitting (hfs) constants for **1** and **2** were firstly calculated using the same model (crystal geometry, B3LYP/TZVP) as for the magnetic measurements. The results listed in Table S2 show a poor agreement with the experimental ones; it is even worse with TVZP/EPR-III. A better agreement is obtained with basis set 6-31*. Therefore, all the further calculations with CH_2Cl_2 as a solvent were performed using the TZVP and 6-31g* sets (Table 4) It can be seen that for the three paramagnetic species a good agreement is obtained with the 6-31g* basis which have also the advantage of requiring short calculation times.

Table 4. Calculated isotropic hyperfine splitting constants (G) for the three paramagnetic species optimized in DCM, using the uB3LYP functional and two basis sets, TZVP, and 6-31g*.

	$\|a_N\|$	HL		**1**		**2**	
	(exp)	TZVP	6-31g*	TZVP	6-31g*	TZVP	6-31g*
a_{N1}	7.40	5.33	7.68	-4.98	-7.22	5.12	7.46
a_{N2}	7.50	5.06	7.59	-4.95	-7.40	5.23	7.79

In conclusion, we described dscribed two new metal-radical complxes, using for the first time, as a ligand, a nitronyl-nitroxid radical derived from *o*-vanillin. The EPR spectra of the nickel complex recorded at two different temperatures clearly show the $S = ½$ ground state, in line with thee magnetic susceptibility measurements and theoretical calculations.

ACKNOWLEDGMENTS

We are thankful to Anamaria Hanganu for NMR spectra recording. Also, we are grateful to Gabriel Crăciun and Adrian Apostol for EDX measurements.

REFERENCES

[1] D. Luneau, *Eur. J. Inorg. Chem*., **2020**, 597 (2020); (b) S. Demir, I.-R. Jeon, J.R. Long, T.D. Harris, *Coord. Chem. Rev*., **289-290**, 149 (2015); (c) X. Meng, W. Shi, P. Cheng, *Coord. Chem. Rev*., **378**, 134 (2019); (d) M.T. Lemaire, *Pure Appl. Chem*., **76**, 277 (2004); (e) C. Benelli, D. Gatteschi, *Chem. Rev*., **102**, 2369 (2002); (f) D. Luneau, P. Rey, *Coord. Chem. Rev.*, **249**, 2591 (2005); (g) A. Caneschi, D. Gatteschi, R. Sessoli, P. Rey, *Acc. Chem. Res.,* **22**, 392 (1989).

[2] J.H. Osiecki, E.F. Ullman, *J. Am. Chem. Soc*., **90**, 1078 (1968); (b) E.F. Ullman, L. Call, J.H. Osiecki, *J. Org. Chem*., **35**, 3623 (1970); (c) E.F. Ullman, J.H. Osiecki, D.G.B. Boocock, R. Darcy, *J. Am. Chem. Soc*., **94**, 7049 (1972); (d) C. Hirel, K.E. Vostrikova, J. Pécaut, V.I. Ovcharenko, P. Rey, *Chem. Eur. J*., **7**, 2007 (2001).

[3] See, for example: (a) J. Sun, Z. Sun, L. Li, J.-P. Sutter, *Inorg. Chem*., **57**, 7507 (2018); (b) G.P. Guedes, R.G. Zorzanelli, N.M. Comerlato, N.L. Speziali, S. Santos-Jr., M.G.F. Vaz, *Inorg. Chem. Commun*., **23**, 59 (2012); (c) H. Miao, M. Li, H.-Q. Li, F.-X. Shen, Y.-Q. Zhang, X.-Y. Wang, *Dalton Trans*., **48**, 4774 (2019); (d) Y.-F. Wang, L.-Y. Wang, L.-F. Ma, *Z. Anorg. Allg. Chem.*, **634**, 181 (2008); (e) P. Y. Chen, M. Z. Wu, T. Li, X. J. Shi, L. Tian, Z. Y. Liu, *Inorg. Chem*., **57**, 12466 (2018); (f) P. Hu, X. Wang, Y. Ma, Q. Wang, L. Li, D. Liao, *Dalton Trans*., **43**, 2234 (2014); (g) J. Omata, T. Ishida, D. Hashizume, F. Iwasaki, T. Nogami, *Inorg. Chem*., **40**, 3954 (2000); (h) Z. Liu, Z. Lu, D. Zhang, Z. Jiang, L. Li, C. Liu, D. Zhu, *Inorg. Chem*., **43**, 6620 (2004); (i) F. Furui, S. Suzuki, M. Kozaki, D. Shiomi, K. Sato, T. Takui, K. Okada, E.V. Tretyakov, S.E. Tolstikov, G.V. Romanenko, V.I. Ovcharenko, *Inorg. Chem*., **53**, 802 (2014); (j) A. Lannes, M. Intissar, Y. Suffren, C. Reber, D. Luneau, *Inorg. Chem.*, **53**, 9548 (2014); (k) J. Guo, J. Sun, G. Sun, Z. Sun, L. Li, *Eur. J. Inorg. Chem*., **2018**, 3241 (2018);

[4] See, for example: (a) L.B.L. Escobar, G.P.Guedes, S. Soriano, N.L. Speziali, A.K. Jordão, A.C. Cunha, V.F. Ferreira, C. Maxim, M.A. Novak, M. Andruh, M.G.F. Vaz, *Inorg. Chem*., **53**, 7508, (2014); (b) M. Zhu, L. Li, J.-P. Sutter, *Inorg. Chem. Front*., **3**, 994 (2016); (c) L. Xi, J. Suan, K. Wang, J. Lu, P. Jing, L. Li, *Dalton Trans*., **49**, 1089, (2020); (d) G. Novitchi, S. Shova, Y. Lan, W. Wernsdorfer, C. Train, *Inorg. Chem.*, **55**, 12122 (2016); (e) A.A. Patrascu, S. Calancea, M. Briganti, S. Soriano, A.M. Madalan, R.A.A. Cassaro, A. Caneschi, F. Totti, M.G.F. Vaz, M. Andruh, *Chem. Commun.*, **53**, 6504 (2017); (f) A. A. Patrascu, M. Briganti, S. Soriani, S. Calancea, R. A. A. Cassaro, F. Totti, M. G. F. Vaz, M. Andruh, *Inorg. Chem*., **58**, 13090 (2019).

[5] M. Andruh, *Dalton Trans*., **44**, 16633 (2015).

[6] A. Vega, J. Padilla, M.A. Leyva, M. del Jesús Rosales, S. Bernès, *J. Mex. Chem. Soc.*, **52**, 54 (2008).

[7] V. Ovcharenko, O. Kuznetsova, E. Fursova, G. Letyagin, G. Romanenko, A. Bogomyakov, E. Zueva*, Inorg. Chem.*, **56**, 14567 (2017).

[8] R. Sayre, *J. Am. Chem. Soc.*, **77**, 6689 (1955).

[9] (a) D.A. Davis, A. Hamilton, J. Yang, L.D. Cremar, D.V. Gough, S.L. Potisek, M.T. Ong, P.V. Braun, T.J. Martinez, S.R. White, J.S. Moore, N.R. Sottos, *Nature*, **459**, 68

(2009); (b) S.S. Deshpande, M.A. Jachak, S.S. Khopkar, G.S. Shankarling, *Sens. Actuators, B*, **258**, 648 (2018).

[10] (a) G.M. Sheldrick, *Acta Cryst*., **A71**, 3-8 (2015); (b) G.M. Sheldrick, *Acta Cryst*., **C71**, 3-8 (2015).

[11] S. Shimono, R. Tamura, N. Ikuma, T. Takimoto, N. Kawame, O. Tamada, N. Sakai, H. Matsuura, J. Yamauchi, *J. Org. Chem.*, **69**, 475 (2004).

[12] M.J. Frisch, G.W. Trucks, H.B. Schlegel, G.E. Scuseria, M.A. Robb, J.R. Cheeseman, G. Scalmani, V. Barone, B. Mennucci, G.A. Petersson, H. Nakatsuji, M. Caricato, X. Li, H.P. Hratchian, A.F. Izmaylov, J. Bloino, G. Zheng, J.L. Sonnenberg, M. Hada, M. Ehara, K. Toyota, R. Fukuda, J. Hasegawa, M. Ishida, T. Nakajima, Y. Honda, O. Kitao, H. Nakai, T. Vreven, J. A. Montgomery, J.E. Peralta, F. Ogliaro, M. Bearpark, J. J. Heyd, E. Brothers, K.N. Kudin, V.N. Staroverov, R. Kobayashi, J. Normand, K. Raghavachari, A. Rendell, J.C. Burant, S.S. Iyengar, J. Tomasi, M. Cossi, N. Rega, J. M. Millam, M. Klene, J.E. Knox, J.B. Cross, V. Bakken, C. Adamo, J. Jaramillo, R. Gomperts, R.E. Stratmann, O. Yazyev, A.J. Austin, R. Cammi, C. Pomelli, J.W. Ochterski, R.L. Martin, K. Morokuma, V.G. Zakrzewski, G.A. Voth, P. Salvador, J.J. Dannenberg, S. Dapprich, A.D. Daniels, O. Farkas, J.B. Foresman, J.V. Ortiz, J. Cioslowski, D.J. Fox, *GAUSSIAN 09, Revision C.01, Gaussian, Inc.*, *Wallingford CT* (2009).

[13] F. Weigend, R. Ahlrichs, *Phys. Chem. Chem. Phys.*, **7**, 3297 (2005).

[14] A.D. Becke, *J. Chem. Phys*., **98**, 5648 (1993).

[15] Y. Wang, J.P. Perdew, *Phys. Rev*., **B 44**, 13298 (1991)**.**

[16] a) Y. Zhao, D.G. Truhlar, *Theor. Chem. Acc.* **120**, 215 (2008); b) R. Valero, R. Costa, I. de P.R. Moreira, D.G. Truhlar, F. Illas, *J. Chem. Phys.*, **128**, 114103-1 (2008).

[17] (a) L. Hermosilla, J.M. Garcia de la Vega, C. Sieiro, P. Calle, *J. Chem. Theory Comput.*, **7**, 169 (2011); (b) L. Hermosilla, P. Calle, J.M.G. de la Vega, C. Sieiro, *J. Phys. Chem. A*, **110**, 13600 (2006); (c) A. Tanaka, K. Nakashima, *Magn. Reson. Chem.* **49**, 603 (2011); (d) C. Zhao, R. Dao, Y. Wang, J. Yao, H. Li, *Chem. Phys.*, **517**, 13 (2019); (e) L. Hermosilla, P. Calle, J.M. García de la Vega, RSC *Advances* **5**, 62551 (2015); (f) O.I. Gromov, S.V. Kuzin, E.N. Golubeva, *J. Mol. Model.*, **25**, 93 (2019).

[18] (a) D. Luneau, F.M. Romero, R. Ziessel, *Inorg. Chem*., **37**, 5078 (1998); (b) C. Stroh, E. Belorizky, P. Turek, H. Bolvin, R. Ziessel, *Inorg. Chem*., **42**, 2938 (2003); (c) C. Aoki, T. Ishida, T. Nogami, *Inorg. Chem*., **42**, 7616 (2003); (c) G. Francese, F.M. Romero, A. Neels, H. Stoeckli-Evans, S. Decurtins, *Inorg. Chem*., **39**, 2097 (2000); (d) U. Schatzschneider, T. Weyhermüller, E. Rentschler, *Eur. J. Inorg. Chem*., **2001**, 2569 (2001); (e) K.E. Vostrikova, E. Belorisky, J. Pécaut, P. Rey, *Eur. J. Inorg. Chem*., **1999**, 1181 (1999); (f) T. Yoshida, T. Suzuki, K. Kanamori, S. Kaizaki, *Inorg. Chem*., **38**, 1059, (1999).

[19] E. Ruiz, J. Cano, S. Alvarez, P. Alemany*, J. Comput. Chem.*, **20**, 1391 (1999).

[20] (a) Z.-H. Zhang, S.-Y. Wu, P. Xu, L-L Li, *Braz. J. Phys.*, **40**, 361 (2010)**;** (b) R. Srinivasan, I. Sougandi, R. Venkatesan, P. S. Rao, *Proc. Indian Acad. Sci. (Chem. Sci.)*, **115**, 91 (2003).

Supporting information

Synthesis, crystal structure, magnetic, spectroscopic, and theoretical investigations of two new nitronyl-nitroxide complexes

Cristian A. Spinu[a], Céline Pichon[b], Gabriela Ionita[c], Teodora Mocanu[a,d], Sergiu Calancea[a,e], Mihai Raduca[a], Jean-Pascal Sutter[c], Mihaela Hillebrand[f] and Marius Andruh[a]

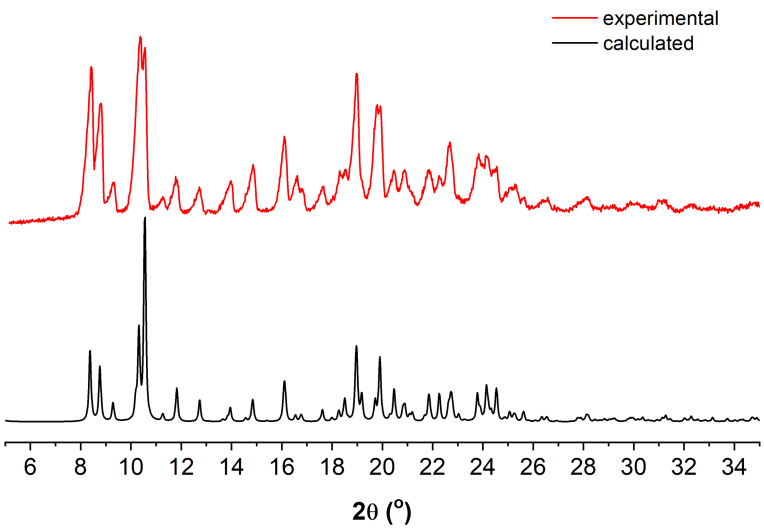

Figure S1. Measured (red) and calculated (black) powder X-ray diffraction patterns of **1**.

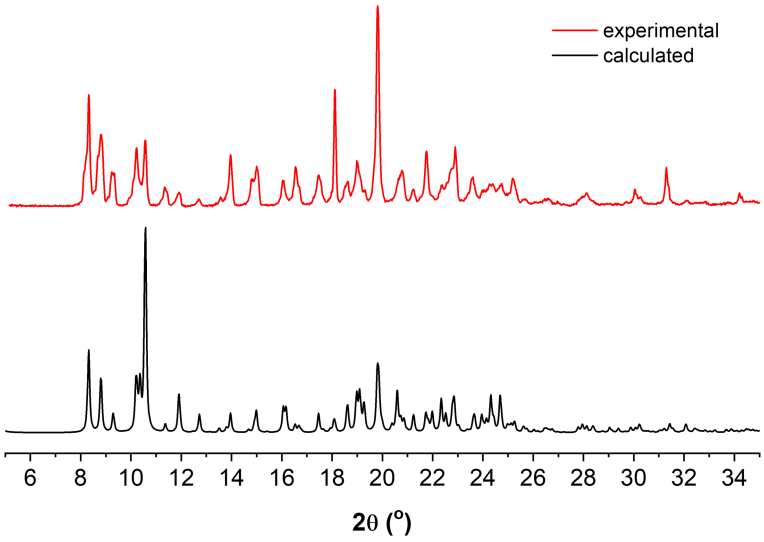

Figure S2. Measured (red) and calculated (black) powder X-ray diffraction patterns of **2**.

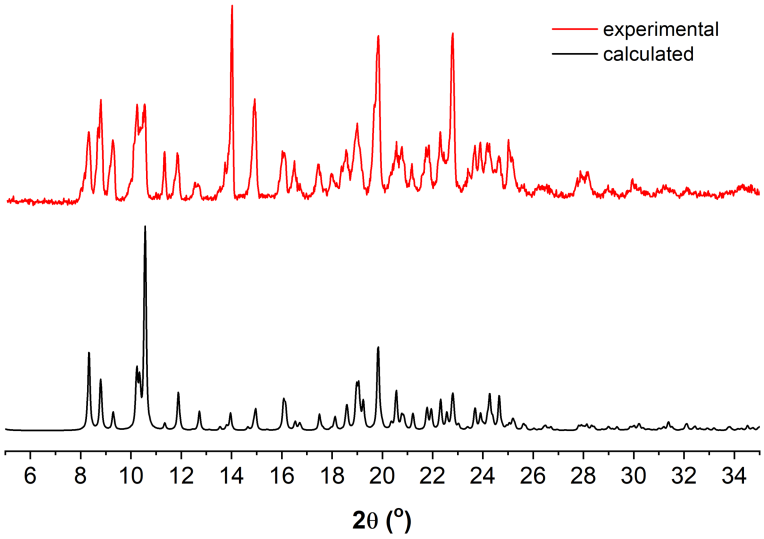

Figure S3. Measured (red) and calculated (black) powder X-ray diffraction patterns of $[Ni_{0.2}Zn_{0.8}]$. The simulated diffractogram was obtained using single crystal measurements of a crystal separated from $[Ni_{0.2}Zn_{0.8}]$.

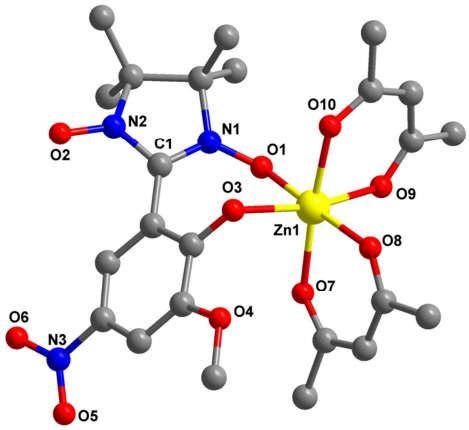

Figure S4. Crystal structure of complex **2**. Hydrogen and fluorine atoms have been omitted for clarity.

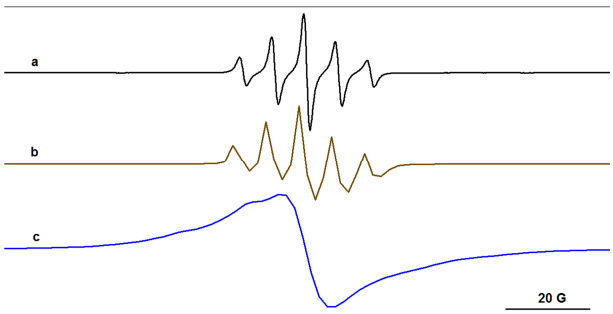

Figure S5. The EPR spectra (in CH_2Cl_2) of a) HL recorded at 293 K, b) complex **2** recorded at 293 K, c) complex **2** recorded at 120 K.

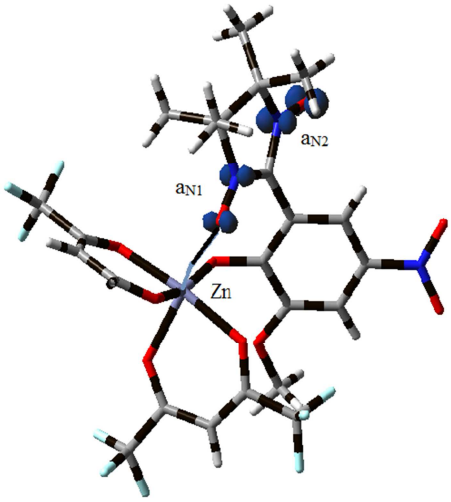

Figure S6. The isodensity (0.04 e^-/(a.u.)^3) surface of complex **2** calculated in DCM at the B3LYP/6-31g* level.

Table S1. Crystallographic data, details of data collection and structure refinement parameters for $[Ni_{0.2}Zn_{0.8}]$.

Complex	**$[Ni_{0.2}Zn_{0.8}]$**
Empirical formula	$C_{30}H_{35}N_4Ni_{0.2}Zn_{0.8}O_{10}F_{12}$
Formula weight	903.66
Temperature (K)	293.15
Crystal system	Monoclinic
Space group	$P2_1/c$
a (Å)	20.3978(8)
b (Å)	9.5639(2)
c (Å)	21.5481(8)
α (°)	90
β (°)	111.215(4)
γ (°)	90
Volume (Å^3)	3918.8(2)
Z	4
D_c (g/cm^3)	1.532
Absorption coefficient (mm^{-1})	0.714
$F(000)$	1842.0
Θ range for data collection (°)	2.142 to 30.746
Index ranges	$-27 \le h \le 27$, $-10 \le k \le 13$, $-27 \le l \le 28$
Reflections collected	38210
Independent reflections [R_{int}]	9784 [R_{int} = 0.0305]
Completeness to Θ full (%)	99.99
Data/restraints/parameters	6784/24/657
Goodness of fit on F^2	0.938
R_1, wR_2 [$I > 2\sigma I$]	0.0402, 0.1237
R_1, wR_2 (all data)	0.0680, 0.1428
Largest diff. peak/hole (Å^3)	0.26/-0.21

Table S2. Hfs constants for complexes **1** and **2** calculated at the uB3LYP level and three basis sets, TZVP,TZVP/EPR-III, 6-31g* considering the crystal geometry.

	$\lvert a_N \rvert$ (exp)	**1**			**2**		
		TZVP	TZVP, EPR-III	6-31g*	TZVP	TZVP, EPR-III	6-31g*
a_{N1}	7.4	-4.37	-3.23	-5.61	4.61	2.29	6.72
a_{N2}	7.5	-4.56	-2.89	-6.55	5.18	3.18	7.70